

Study of the reaction $\pi^- p_{\uparrow} \rightarrow \pi^- \pi^+ n$ on the polarized proton target at 1.78 GeV/c. Experiment and amplitude analysis.

I.G. Alekseev, P.E. Budkovsky, V.P. Kanavets, L.I. Koroleva,
I.I. Levintov, V.I. Martynov, B.V. Morozov, V.M. Nesterov,
V.V. Ryltsov, D.N. Svirida, A.D. Sulimov, V.V. Zhurkin

*Institute for Theoretical and Experimental Physics,
B. Chermushkinskaya 25, Moscow, 117259, Russia
Tel: 7(095)123-80-72, Fax: 7(095)127-08-33
E-mail : kanavets@vitep5.itep.ru*

V.V. Sumachev

*Petersburg Nuclear Physics Institute,
Gatchina, Leningrad district, 188350, Russia*

Abstract

We present the results of the experimental study of the reaction of dipion production by the beam of the negative pions with momentum 1.78 GeV/c on the polarized proton and liquid hydrogen targets. The experiment covers the region of dipion masses near the mass of ρ -meson and small momenta transferred $|t| < 0.2$ (GeV/c)². The whole set of spin density matrix elements was reconstructed and model-independent and model-dependent amplitude analyses of the reaction were performed. The experiment allows to exclude the ambiguity of the amplitude analysis existing at high energies. The results contain evidences in favour of existing of narrow $\sigma(750)$ 00^{++} . The data also allows to estimate intercept of a_1 -meson Regge trajectory.

The experiment was performed at the ITEP proton synchrotron, Moscow.

PACS number(s) : 13.75.Gx, 13.88.+e.

Key words: amplitude analysis, polarized proton target, rho-meson, scalar mesons, spin density matrix elements,

1 Introduction

Exclusive reactions of pion production are an important source of information on the nature of the strong interaction. They allow to study the dynamics of the processes as well as the pion-pion interaction. Up to now a number of experiments which study production of pions by pions were fulfilled on unpolarized proton targets [1–7] in the intermediate energy region. Their results showed the predominant role of the one pion exchange (OPE) and noticeable effects of absorption. The whole picture was satisfactorily described by models of the one pion exchange with absorption (OPEA) [8] and Regge-model with moving branchings [9]. Nevertheless the absence of information on the spin dependence of the reaction at the intermediate energies (except the preliminary results of this experiment [10]) did not allow to go further in the understanding of the reaction mechanism, particularly it was not possible to estimate contribution of the axial-vector exchange.

Here we should mention two experiments with transversely polarized targets performed at high energies. Authors of the first experiment [11] used a polarized proton target to study the reaction

$$\pi^- p \rightarrow \pi^+ \pi^- n \quad (1)$$

at the incident pion beam momentum 17.2 GeV/c. In the other [12] the reaction

$$\pi^+ n \rightarrow \pi^+ \pi^- p \quad (2)$$

was explored at 5.98 and 11.85 GeV/c on a polarized deuteron target. In both experiments large asymmetries (up to 50%) in the ρ -meson production were observed. This was explained as a result of the essential contribution of the axial-vector exchange (a_1 -meson), that caused doubts about the results of partial wave analyses, which neglected this mechanism. Untrivial results of these experiments put forward the question of the energy dependence of the asymmetries. The latter would allow to estimate intercept of axial-vector Regge trajectory.

The angular distributions of the products of the reaction (1) at the transversely polarized target allow to fulfill a nearly full model independent amplitude analysis of the reaction [13]. So in the region of the dipion masses below 1 GeV where contribution of waves with $L \geq 2$ is negligible, one can directly reconstruct modules of all the transversity amplitudes and most of the phases. Besides all, this makes possible to separate the intensities of the dipions produced in the S - and P -wave states without additional assumptions and thus

study the mass dependence of S -wave which is important for the scalar meson spectroscopy.

Up to now the main source of information about light quark meson spectroscopy is the partial wave analyses of the pion-pion scattering. Old analyses were based on the data obtained on unpolarized targets. In order to study the pion-pion interaction authors of these works separated the diagram of the one pion exchange and then made a transition from the scattering on the virtual pion to the scattering on the real one [14]. The other method is to perform a partial wave analysis basing on the amplitudes of the reaction. But the model independent amplitude reconstruction is impossible without measurements on polarized targets. In the absence of such data the assumption was used that in the helicity system one could disregard amplitudes without the nucleon helicity flip [15]. In addition the partial wave analyses used strong but not well proven assumptions of "spin coherence", that is the absence of a_1 exchanges, and "phase coherence", that is the equality of phases of P -waves with zero and unit helicities. On the other hand the analysis of the situation using Roy's equations [16], incorporating conditions of unitarity, analyticity and crossing symmetry, showed that solutions of partial wave analysis are self content and generally correct [17], though individual analyses had noticeable difference in the S -wave phases.

The results of partial wave analyses had an ambiguity in the behavior of the δ_0^0 phase (S -wave with zero isospin) at dipion masses above 700 MeV, so called "UP-DOWN" ambiguity. The "UP" solution revealed more quick change of the δ_0^0 phase under the peak of ρ -meson and was considered as resonance opposite to the "DOWN" solution. The direct measurements of the mass dependence of the pion-pion interaction intensity with two π^0 -mesons in the final state did not lead to a clear conclusion about the existence of the relatively narrow scalar resonance [18,19]. The experiments at high energies with polarized targets [11,12] showed large polarization effects that contradicted to the assumptions on which partial wave analyses were based. The model-independent amplitude analysis of the data from [11,12] performed by M. Svec in [20] gave 4-fold ambiguity in the solution, but all the variants corresponded to the resonant behaviour of the S -wave in the ρ -meson region. The important additional argument in favour of the existence of the resonance, obtained in this analysis, is the weak mass dependence of the relative phase between S -wave and P -wave with zero helicity. The simultaneous amplitude analysis of the reaction (1) together with the reaction $\pi^+p \rightarrow \pi^+\pi^-\Delta^{++}$ [21] gave two branches of the solution. One corresponded to a relatively narrow resonance ($M = 750$ MeV and $\Gamma = 200$ MeV) and the other — to a wide one ($M = 600$ MeV and $\Gamma = 450$ MeV). The recent partial wave analysis of the data [11], which took into account the axial-vector exchange, gave also two branches of the solution for the phase δ_0^0 [22]. So the current amount of the experimental data over peripheral meson production is not sufficient

to solve the "UP-DOWN" ambiguity, which preserves the open problem in the meson spectroscopy. Nevertheless this data points out to the existence of the scalar-isoscalar resonance in the mass region below 1 GeV (wide sigma-meson $f_0(400 - 1200)$ and/or narrow $f_0(750)$). The history of the search of the scalar-isoscalar meson is long and contradictory. The σ -meson was for the first time proposed in the work [23]. Up to 1974 this resonance was present in the PDG tables as σ , ϵ or δ_{0+} . In 1996 it again appeared in PDG tables [24] as $f_0(400 - 1200)$.

Thus the modern state of the problem of light scalar-isoscalar meson requires additional experimental information and to provide such information was one of the goals of this work. We present here a new experimental data on the reaction (1) on the polarized proton and liquid hydrogen targets in the region of small momentum transferred at $p_{\text{beam}} = 1.78$ GeV/c. The results are compared with the ones at high energies ($p_{\text{beam}} = 17.2$ GeV/c [11,20]). The results are analyzed with the help of the Regge phenomenology, which gives the natural connection between the high and intermediate energy regions.

2 Basic formalism

Here we only want to review the basic formalism which could be found elsewhere in more details [20,25–27,13]. At fixed beam momentum the reaction (1) is described by 5 kinematic variables. We use two energy variables (the squared momentum transferred t ¹ and the dipion invariant mass $M_{\pi\pi}$) and three angular variables. One angle ψ describes the reaction plane and is defined as the angle between the normal to the reaction plane and the target polarization P_t . The other two angles describe the dipion decay in its rest frame and are defined as angles θ (Gotfried-Jackson angle) and ϕ (Treiman-Yang angle) of the negative pion in the Jackson coordinate system (helicity system of the t-channel, axis z along the beam and y perpendicular to the reaction plane).

The dynamics of the reaction (1) could be described by the set of the helicity amplitudes $\langle j, m, \chi | T | \lambda \rangle(s, t, M_{\pi\pi})$, where j and m are the spin and the helicity of the dimeson, while χ and λ are the neutron and proton helicities correspondingly. At $M_{\pi\pi} < 1$ GeV the dipion production with spins $j = 0$ (S -wave) and $j = 1$ (P -wave) is dominant. Thus the reaction (1) in the energy region under consideration is described by 8 complex amplitudes: two for dipion production in S -state (with and without neutron helicity flip) and 6 for dipion production in P -state (with dipion helicities $+1, 0, -1$ with or without neutron helicity flip). An experiment with a transversely polarized target

¹ or $t' = t - t_{\text{min}}$ instead of t

yield 15 elements of spin density matrix (SDME) $\rho_{\alpha\beta}(s, t, M_{\pi\pi})$, defining the angular distributions of the reaction products. Nine of them reflect the interference of the helicity flip and non-flip amplitudes and can be measured only in polarized target experiment.

The normalized process intensity as function of the SDME and the angular variables could be written as follows:

$$I(\theta, \phi, \psi) = I_0(\theta, \phi) + P_t \cdot \cos \psi \cdot I_Y(\theta, \phi) + P_t \cdot \sin \psi \cdot I_X(\theta, \phi), \quad (3)$$

where

$$\begin{aligned} I_0(\theta, \phi) = & 1 + (\rho_{00} - \rho_{11}) \cdot (3 \cos^2 \theta - 1) - \\ & \rho_{1-1} \cdot 3 \sin^2 \theta \cos 2\phi - \operatorname{Re} \rho_{10} \cdot 3\sqrt{2} \sin 2\theta \cos \phi - \\ & \operatorname{Re} \rho_{1S} \cdot 2\sqrt{6} \sin \theta \cos \phi + \operatorname{Re} \rho_{0S} \cdot 2\sqrt{3} \cos \theta, \end{aligned} \quad (4)$$

$$\begin{aligned} I_Y(\theta, \phi) = & A + (\rho_{00}^Y - \rho_{11}^Y) \cdot (3 \cos^2 \theta - 1) - \\ & \rho_{1-1}^Y \cdot 3 \sin^2 \theta \cos 2\phi - \operatorname{Re} \rho_{10}^Y \cdot 3\sqrt{2} \sin 2\theta \cos \phi - \\ & \operatorname{Re} \rho_{1S}^Y \cdot 2\sqrt{6} \sin \theta \cos \phi + \operatorname{Re} \rho_{0S}^Y \cdot 2\sqrt{3} \cos \theta, \end{aligned} \quad (5)$$

$$\begin{aligned} I_X(\theta, \phi) = & \operatorname{Im} \rho_{1-1}^X \cdot 3 \sin^2 \theta \sin 2\phi + \operatorname{Im} \rho_{10}^X \cdot 3\sqrt{2} \sin 2\theta \sin \phi + \\ & \operatorname{Im} \rho_{1S}^X \cdot 2\sqrt{6} \sin \theta \sin \phi. \end{aligned} \quad (6)$$

With two additional relations:

$$\rho_{SS} + \rho_{00} + 2\rho_{11} = 1, \quad (7)$$

$$\rho_{SS}^Y + \rho_{00}^Y + 2\rho_{11}^Y = A. \quad (8)$$

The first of them expresses the normalization and the second defines A — conventional polarized target asymmetry.

The data on transversely polarized target is best analyzed in terms of the nucleon transversity amplitudes with definite t-channel exchange naturality : S, L, U, N and $\bar{S}, \bar{L}, \bar{U}, \bar{N}$. These amplitudes are linear combinations of helicity amplitudes and correspond to definite recoil nucleon transversity ("down" and "up" respectively). The amplitudes S, \bar{S} and L, \bar{L} describe production of the S -wave and P -wave dipions with zero helicity, respectively. Amplitudes $S, \bar{S}, L, \bar{L}, U, \bar{U}$ are dominated by unnatural exchange, while amplitudes N, \bar{N} - by natural one.

$$S = \frac{1}{\sqrt{2}}(\langle 0, 0, +|T|+ \rangle + i \cdot \langle 0, 0, +|T|- \rangle), \quad (9)$$

$$\bar{S} = \frac{1}{\sqrt{2}}(\langle 0, 0, +|T|+ \rangle - i \cdot \langle 0, 0, +|T|- \rangle), \quad (10)$$

$$L = \frac{1}{\sqrt{2}}(\langle 1, 0, +|T|+\rangle + i \cdot \langle 1, 0, +|T|-\rangle), \quad (11)$$

$$\bar{L} = \frac{1}{\sqrt{2}}(\langle 1, 0, +|T|+\rangle - i \cdot \langle 1, 0, +|T|-\rangle), \quad (12)$$

$$U = \frac{1}{2}(\langle 1, +1, +|T|+\rangle - \langle 1, -1, +|T|+\rangle + i \cdot \langle 1, +1, +|T|-\rangle - i \cdot \langle 1, -1, +|T|-\rangle), \quad (13)$$

$$\bar{U} = \frac{1}{2}(\langle 1, +1, +|T|+\rangle - \langle 1, -1, +|T|+\rangle - i \cdot \langle 1, +1, +|T|-\rangle + i \cdot \langle 1, -1, +|T|-\rangle), \quad (14)$$

$$N = \frac{1}{2}(\langle 1, +1, +|T|+\rangle + \langle 1, -1, +|T|+\rangle + i \cdot \langle 1, +1, +|T|-\rangle + i \cdot \langle 1, -1, +|T|-\rangle), \quad (15)$$

$$\bar{N} = \frac{1}{2}(\langle 1, +1, +|T|+\rangle + \langle 1, -1, +|T|+\rangle - i \cdot \langle 1, +1, +|T|-\rangle - i \cdot \langle 1, -1, +|T|-\rangle). \quad (16)$$

These amplitudes are connected to SDME by the following equations:

$$\rho_{SS} + \rho_{00} + 2\rho_{11} = |S|^2 + |\bar{S}|^2 + |L|^2 + |\bar{L}|^2 + |U|^2 + |\bar{U}|^2 + |N|^2 + |\bar{N}|^2 = 1, \quad (17)$$

$$\rho_{00} - \rho_{11} = |L|^2 + |\bar{L}|^2 - \frac{1}{2}(|N|^2 + |\bar{N}|^2 + |U|^2 + |\bar{U}|^2), \quad (18)$$

$$\rho_{1-1} = \frac{1}{2}(|N|^2 + |\bar{N}|^2 - |U|^2 - |\bar{U}|^2), \quad (19)$$

$$\text{Re } \rho_{10} = \frac{1}{\sqrt{2}} \text{Re}(UL^* + \bar{U}\bar{L}^*), \quad (20)$$

$$\text{Re } \rho_{0S} = \text{Re}(LS^* + \bar{L}\bar{S}^*), \quad (21)$$

$$\text{Re } \rho_{1S} = \frac{1}{\sqrt{2}} \text{Re}(US^* + \bar{U}\bar{S}^*), \quad (22)$$

$$\rho_{SS}^Y + \rho_{00}^Y + 2\rho_{11}^Y = |S|^2 - |\bar{S}|^2 + |L|^2 - |\bar{L}|^2 + |U|^2 - |\bar{U}|^2 - |N|^2 + |\bar{N}|^2 = A, \quad (23)$$

$$\rho_{00}^Y - \rho_{11}^Y = |L|^2 - |\bar{L}|^2 - \frac{1}{2}(-|N|^2 + |\bar{N}|^2 + |U|^2 - |\bar{U}|^2), \quad (24)$$

$$\rho_{1-1}^Y = -\frac{1}{2}(|N|^2 - |\bar{N}|^2 + |U|^2 - |\bar{U}|^2), \quad (25)$$

$$\text{Re } \rho_{10}^Y = \frac{1}{\sqrt{2}} \text{Re}(UL^* - \bar{U}\bar{L}^*), \quad (26)$$

$$\text{Re } \rho_{0S}^Y = \text{Re}(LS^* - \bar{L}\bar{S}^*), \quad (27)$$

$$\text{Re } \rho_{1S}^Y = \frac{1}{\sqrt{2}} \text{Re}(US^* - \bar{U}\bar{S}^*), \quad (28)$$

$$\text{Im } \rho_{1-1}^X = -\text{Re}(NU^* - \bar{N}\bar{U}^*), \quad (29)$$

$$\text{Im } \rho_{10}^X = \frac{1}{\sqrt{2}} \text{Re}(NL^* - \bar{N}\bar{L}^*), \quad (30)$$

$$\text{Im } \rho_{1S}^X = \frac{1}{\sqrt{2}} \text{Re}(NS^* - \bar{N}\bar{S}^*). \quad (31)$$

It is also useful to introduce partial-wave intensities I_A and partial-wave polarizations P_A :

$$I_A = |A|^2 + |\bar{A}|^2, \quad P_A = |A|^2 - |\bar{A}|^2, \quad (32)$$

where $A = S, L, U, N$.

The absolute values of the transversity amplitudes could be reconstructed from the experiment on a polarized target. This is not so for the helicity amplitudes. The matrix elements measured allow to reconstruct the absolute values of all the amplitudes involved and all relative phases between them, except the relative phase between the two groups of amplitudes with different recoil nucleon transversity. The relations between the SDME and the amplitudes could be put in the form of two independent similar systems of equations [13,20], one for amplitudes S, L, U and \bar{N} and the other for amplitudes with the opposite recoiled nucleon transversity. Each of the systems could be reduced to a cubic equation in respect to $|L|^2$ or $|\bar{L}|^2$, correspondingly, which has two positive solutions. This provides two-fold ambiguity in the resulting amplitudes and four-fold ambiguity in the partial wave intensities.

3 Experimental layout

The apparatus used in this work is the further development of the experimental setup **SPIN** [29,10] designed for the investigation of polarization effects in two- and three-particle reactions with two charged particles in the final state. It is a two-arm magnetic spectrometer with wire chambers and a transversely polarized proton target. Spectrometric capabilities of the setup are provided by the magnet of the polarized target equipped with spark chambers placed in its field. The apparatus is located at the ITEP accelerator in the beam of particles with maximum momentum 2.1 GeV/c. The typical beam intensity is $5 \cdot 10^5$ pions per spill, the spill duration is about 1 s and the frequency is 20–25 spills per minute. The beam angular divergences are ± 6.5 and ± 3.5 mrad in the horizontal and vertical planes respectively. Its dimensions on the target are 8–10 mm in both projections. The momentum spread of the beam is $\pm 2\%$. The central beam momentum was determined with the precision better than 0.5% by bending of the incident particles in the well known magnetic field of

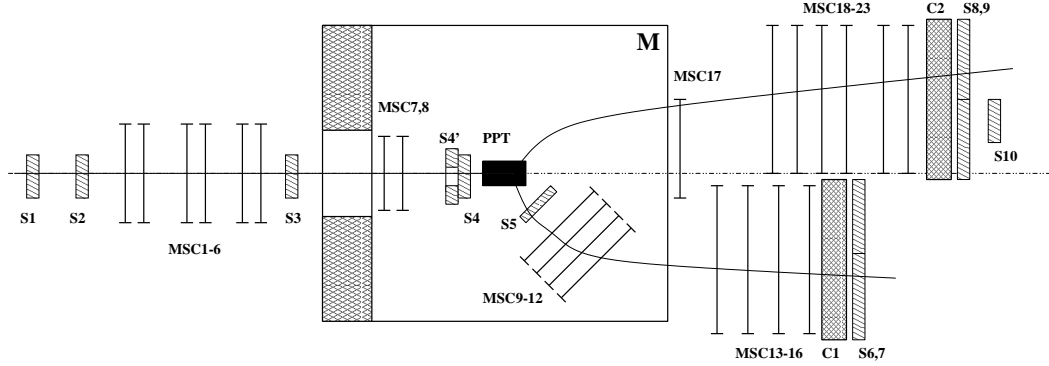


Fig. 1. Experimental layout.

the polarizing magnet and by the time-of-flight difference between negative pions and anti-protons of the beam [30].

The setup **SPIN** is shown in fig. 1. The basic elements are:

- Polarized proton target (**PPT**), placed in the center of a wide aperture magnet (**M**). The magnet (**M**) is C-shaped iron magnet with approximately axially symmetrical horizontal field. The field in the center is 2.55 T with non-uniformity in the region of the target less than $2 \cdot 10^{-4}$. The bending power from the center is 0.45 T·m. The protons of the target are polarized by the dynamic nuclear orientation method. The target material is propanediol $C_3H_8O_2$ doped by HBMA-Cr^V complexes. Target dimensions are $21 \cdot 28 \cdot 60 \text{ mm}^3$ (width·height·length). The working temperature of the target 0.5 K is achieved with a ^3He -evaporation type cryostat. The polarization is measured by the NMR method with the precision of 5%. The average polarization during the data taking was $70 \pm 5\%$.
- Liquid hydrogen target, which can be placed in the same cryostat as the polarized target. This allows to make measurements on both types of targets without additional readjustments of the setup — just by replacing the target. The liquid hydrogen is produced by the cooling of the gaseous hydrogen by the liquid helium at the atmospheric pressure. The helium stream in the heat exchanger was automatically adjusted so as to keep the hydrogen pressure in the closed volume of the target constant. This allows to maintain the volume of the liquid hydrogen with the precision better than 2%.
- Wire spark chambers with magnetostrictive readout (**MWSC1–23**), which allow to measure trajectories of the incoming pion (**MWSC1–8**) and two outgoing charged particles: (**MWSC9–16**) in the lower arm and (**MWSC17–23**) in the upper arm. The chambers (**MWSC9–12**) of the lower arm placed into the magnetic field provide the spectrometric capabilities of the apparatus.
- System of scintillation and Cherenkov counters (**S1–10** and **Ĉ1,2**) for triggering. The threshold Cherenkov counters provide suppression of protons and are used in the trigger, which was formed according to the equation:

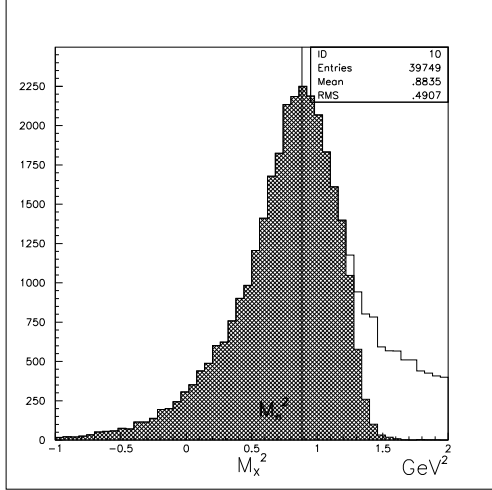


Fig. 2. Events distribution over missing mass squared.

$$\text{Trig.} = S1 \cdot S2 \cdot S3 \cdot S4 \cdot \overline{S4'} \cdot \check{C}1 \cdot \check{C}2 \cdot \overline{S10} \cdot (S6 + S7) \cdot (S8 + S9) , \quad (33)$$

where veto counter **S10** is placed on the continuation of the beam line after the magnet.

The adjustment of the apparatus was performed in two subsidiary runs. In one of them the special copper wire target was used to produce events with known vertex coordinates and in the other the beam which momentum was controlled with time-of-flight technique was bended by the magnet into different arms of the setup.

4 Data processing

Data processing was performed in two stages. At the first stage the kinematic parameters of the individual events were reconstructed. For every event the interaction point and particles momenta as well as their error matrixes were reconstructed taking into account multiple scattering in the materials of the setup [31]. The final kinematic parameters were found using the hypothesis that the missing particle is a neutron. The distribution of the events over missing mass squared is shown in fig. 2 (solid line). Further event selection was based on the χ^2 of the hypothesis that the missing particle is a neutron. We assumed that in the background events one or more missed pions are produced and then the missing mass in such events should be greater the mass of a neutron. We made processing with different rejections over χ^2 and missing mass and found no significant difference. Finally we rejected events whose missing mass was above the mass of nucleon and $\chi^2 > 5$. In fig. 2 “Good” events are shown by hatched area. The event distributions over momentum

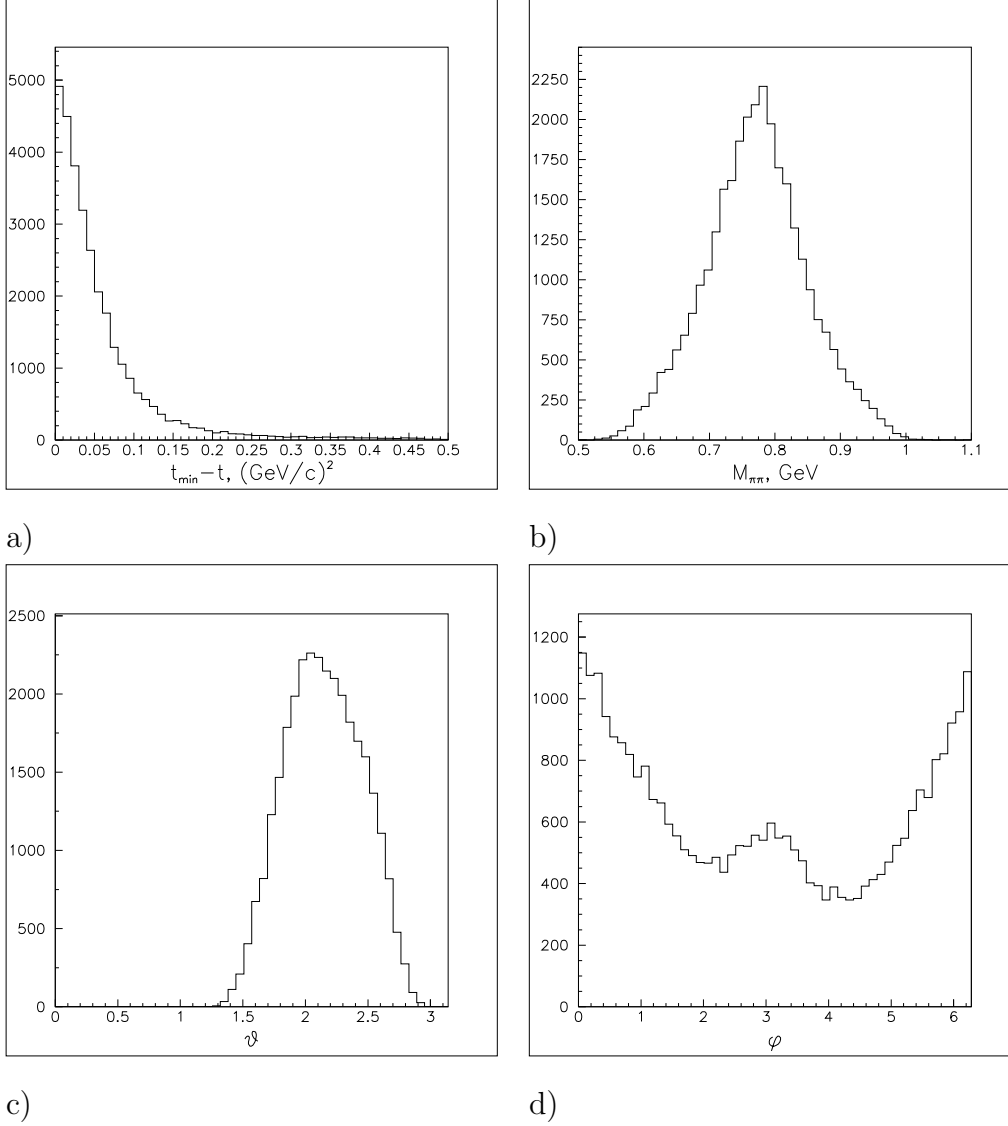


Fig. 3. Events distributions over momentum transferred $t_{\min} - t$ (a), dipion invariant mass $M_{\pi\pi}$ (b), Gottfried-Jackson angle θ (c) and Treiman-Yang angle ϕ (d).

transferred $t_{\min} - t$, dipion invariant mass $M_{\pi\pi}$, Gottfried-Jackson angle θ and Treiman-Yang angle ϕ on the liquid hydrogen target are shown in fig. 3. These figures describe the kinematic region covered by the setup.

At the second stage the SDME of the reaction were reconstructed using the method of maximum likelihood [32] in bins over dipion mass and momentum transferred. For a given angular distribution of the events $I(\theta, \phi, \psi)$ the likelihood function could be expressed as a product over all the events observed :

$$L = \prod_i^N \{I(\theta_i, \phi_i, \psi_i) \cdot \eta(\theta_i, \phi_i, \psi_i)/C\}, \quad (34)$$

where N is the total number of events, $\eta(\theta_i, \phi_i, \psi_i)$ — the probability of the apparatus to count the event with given kinematic parameters and C is normalizing constant which is defined as the integral:

$$C = \int I(\theta_i, \phi_i, \psi_i) \cdot \eta(\theta_i, \phi_i, \psi_i) \cdot d\Omega, \quad (35)$$

which is taken over the whole phase space and can be found using Monte-Carlo technique as a sum over all events hitting the modelled setup:

$$C = \frac{1}{K} \sum_i^K I(\theta_i, \phi_i, \psi_i), \quad (36)$$

here K is the number of Monte-Carlo events. We searched for a maximum of the function

$$\ln L = \sum_i^N \ln I(\theta_i, \phi_i, \psi_i) + \sum_i^N \ln \eta(\theta_i, \phi_i, \psi_i) - N \cdot \ln C. \quad (37)$$

The second term does not depend upon the SDME and can be omitted. The Monte-Carlo simulation was performed with the aid of the GEANT code [33]. The method of effective sample [34] was used to reduce the computer time required. According to this method the events were simulated with different probabilities over $M_{\pi\pi}$ and t' , so that distributions of simulated events reminded the experimental distributions. Then the sum in (36) was calculated with necessary correction. The results of Monte-Carlo simulations were also used to ensure our understanding of apparatus acceptance and errors and to test program of event reconstruction: (i) we compared simulated distributions with real ones using reconstructed SDME; (ii) the Monte-Carlo generated events were processed by the program of event reconstruction and reconstructed parameters were compared to generated ones; (iii) missing mass squared distribution of Monte-Carlo events after reconstruction was built.

The uncertainty in the missing mass does not allow to separate the reaction on the free protons from the background reactions on the protons bound in the nuclei of the target material. So we determined the spin-independent SDME in the experiment on liquid hydrogen target only. The spin-dependent SDME were determined from the data, obtained in the experiment on the polarized proton target, in two-step processing. On the first step the spin-independent SDME on the target material mixture of nucleus were found. Then the spin-dependent SDME on the polarized hydrogen of the target were determined. To equalize the data samples with different target polarization the weight

Table 1

Polarization dissolution factor

$M_{\pi\pi}$, GeV	k
0.65–0.75	3.6 ± 0.2
0.75–0.80	2.8 ± 0.2
0.80–0.90	4.3 ± 0.4

function

$$\frac{w_-}{w_+} = \sqrt{\frac{N_{\uparrow}^+ \cdot N_{\downarrow}^+}{N_{\uparrow}^- \cdot N_{\downarrow}^-}} \quad (38)$$

was used [35]. Here w^\pm are the weights attributed to the events with corresponding target polarization and $N_{\uparrow\downarrow}^\pm$ — numbers of the events with positive or negative target polarization and in which dipion goes up or down correspondingly.

The spin-dependent data obtained on polarized target is averaged by the whole nuclei mixture of the target material. The correction for this effect was made by polarization dissolution factor, given in the table below. The factor was calculated from beam monitor counts, chamber efficiencies and spin-independent SDME.

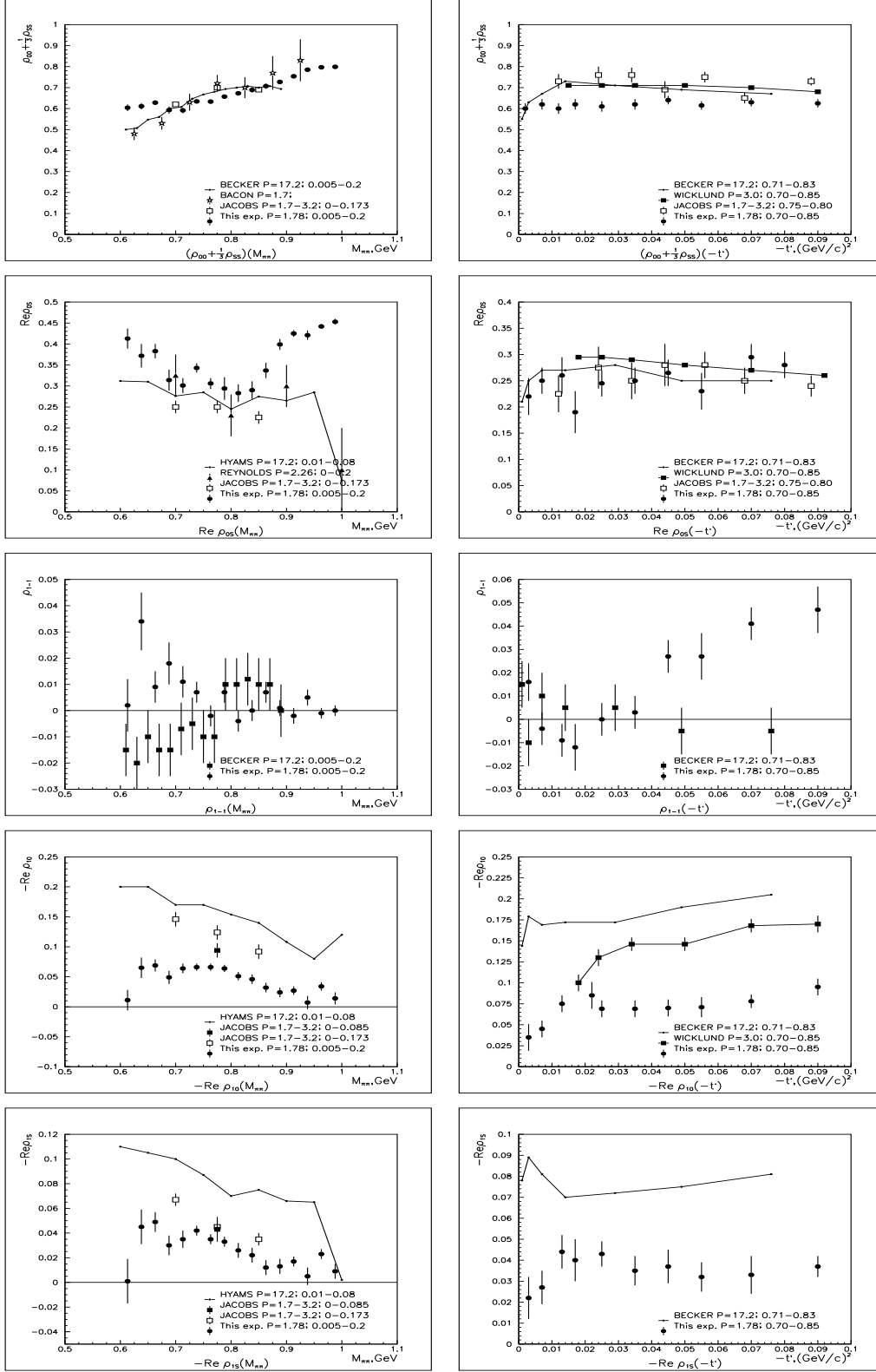
5 Results

The statistics (after event reconstruction) is $40 \cdot 10^3$ events on LH_2 target and about $320 \cdot 10^3$ events on the polarized target in the kinematic range $0.005 < t' < 0.2$ (GeV/c)² and $0.6 < M_{\pi\pi} < 1.0$ GeV.

5.1 Spin-independent SDME

The normalized spin-independent SDME in the t-channel system (Jackson frame) are presented in fig. 4 as functions of dipion mass $M_{\pi\pi}$ and momentum transferred $-t'$. Numeric data is given in the appendix.

The matrix element $\rho_{00} + \frac{1}{3}\rho_{SS}$ measured in all the experiments show approximately the same behavior as a function of the dipion mass. The matrix element $\text{Re } \rho_{0S}$ in our experiment at $M_{\pi\pi} > 0.85$ GeV significantly differs from the data at the high energies. This probably could be attributed to the asymptotically vanishing amplitudes containing a term $\sqrt{\frac{t_{\min}}{t'}}$, which quickly increases when



a)

b)

Fig. 4. Spin-independent density matrix elements as function of dipion invariant mass $M_{\pi\pi}$ (a) and momentum transferred $-t'$ (b).

$M_{\pi\pi}$ goes toward 1 GeV. The matrix element ρ_{1-1} is small, as it is at high energies. The matrix elements $\text{Re } \rho_{10}$ and $\text{Re } \rho_{1S}$ are decreasing in the mass range (0.8–0.9) GeV essentially quicker than at high energies. These SDME also show obvious energy dependence. The standard description of the dipion production in the frame of the one pion exchange with absorption (OPEA) model [8] gives the following mass dependence of the matrix element ratios:

$$\frac{\text{Re } \rho_{10}}{\rho_{00} - \rho_{11}} = \frac{\text{Re } \rho_{1S}}{\text{Re } \rho_{0S}} = -\frac{\text{const.}}{M_{\pi\pi}}. \quad (39)$$

The experimental data qualitatively follows the equation, but demonstrates stronger dipion mass dependence in the range (0.7–0.95) GeV.

Let us assume a small relative phase between S and L waves and take the experimental data for the values of the SDME $\rho_{00} + \frac{1}{3}\rho_{SS}$, $\text{Re } \rho_{0S}$ and ρ_{1-1} . Then we can use equations (17-22) connecting amplitudes to the SDME to show that in these conditions intensity of the U -wave decreases 3 times in the dipion mass region (0.8–0.92) GeV, that agree with the strong mass dependence of SDME $\text{Re } \rho_{10}$ and $\text{Re } \rho_{1S}$. We will show below that the assumption about the phases corresponds to the only physically justified solution of the amplitude analysis.

The behavior of the t' -dependencies is similar to those at high energies. All SDME but ρ_{1-1} show no significant dependence over t' at $-t' > 0.01$. At t' near zero the expected kinematic suppression of $\text{Re } \rho_{10}$ and $\text{Re } \rho_{1S}$ is observed. The matrix element ρ_{1-1} has a slow growth up to $-t' = 0.1$ that agree with the predictions of the Regge model with moving branchings [9]. The data does not exclude a slight energy dependence of $\rho_{00} + \frac{1}{3}\rho_{SS}$.

5.2 Spin dependence of the reaction

The preliminary estimation of the asymmetry could be done using the function

$$E(\psi) = \frac{N^+(\psi) - N^-(\psi)}{N^+(\psi) + N^-(\psi)}, \quad (40)$$

where N^+ , N^- are the normalized counts of the setup for positive and negative target polarization. The fit with the cosine function of the experimental values of $E(\psi)$ is shown in fig. 5. The spin dependence of the reaction is seen at the level of $6 \cdot \sigma_{\text{stat}}$. Assuming only the asymmetry and no other terms in (5) and making corrections for the mean target polarization and the dissolving effect on unpolarized complex nuclei of the target one can found that this

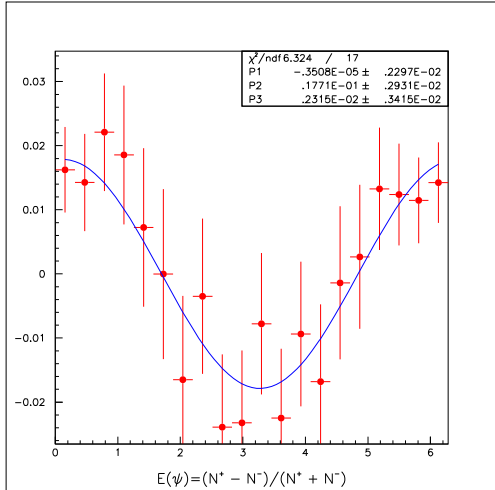


Fig. 5. Raw asymmetry (40) as function of the angle ψ .

fit corresponds to asymmetry about 9% with the same sign as at the high energies.

Only four SDME, namely $A = \rho_{SS}^Y + \rho_{00}^Y + 2\rho_{11}^Y$, $\rho_{00}^Y - \rho_{11}^Y$, $\text{Re } \rho_{10}^Y$ and $\text{Im } \rho_{10}^X$ turned out to be nonzero within the experimental errors. They are shown in fig. 6 in comparison with the data at 17.2 GeV/c [11] and listed in the appendix. The signs of spin-dependent SDME coincide with those at high energies but the absolute values are significantly smaller.

We would like to draw attention to the nonzero value of the SDME $\text{Im } \rho_{10}^X$, which describes interference between the waves with different naturality (see equation (30)). This fact evidences in favour of the contribution of amplitudes with natural parity and the phase different from the phase of leading (L, \bar{L}) amplitudes. In the frame of Regge model this corresponds to the contribution of a_2 -Regge trajectory (a_2 -meson has $J^P = 2^+$).

5.3 Amplitude analysis

The results of the model-independent amplitude analysis of the reaction are shown in fig. 7,8 in comparison with the results at 17.2 GeV/c from the analysis [20]. The analysis was performed in 25 MeV bins over dipion mass. The polarization data was taken constant within wider bins in which it was available.

Our model-independent analysis produced two significantly different solutions 1 and 2. At all energies (1.78, 5.98, 11.85 and 17.2 GeV/c) where model-independent analyses were performed they resulted in two-fold ambiguity solutions with the same clear signatures. The solution 1 gives a very small angle

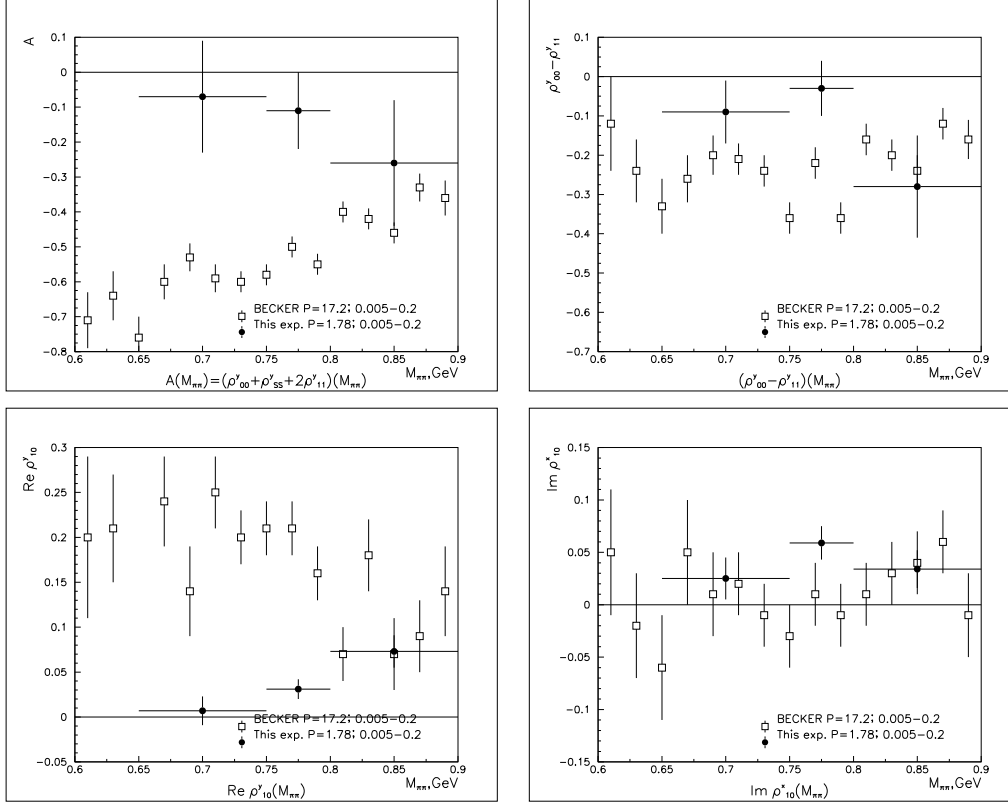
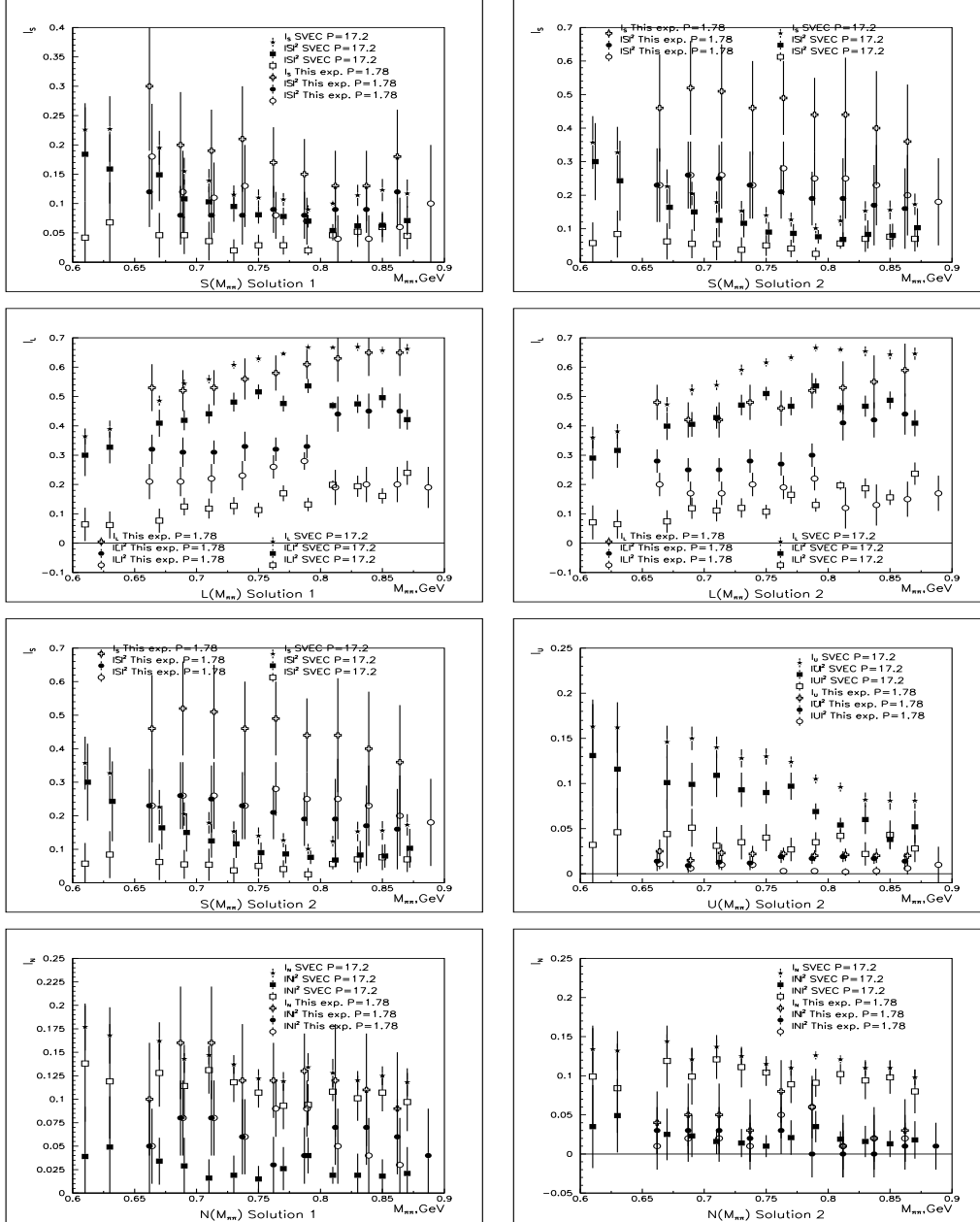


Fig. 6. Spin-dependent density matrix elements. Full dots — this experiment, open squares — Becker et al. [11].

between S and L -waves and the solution 2 gives an angle between L and U -waves near 180° independently of the recoil nucleon transversity. In addition the solution 1 has essentially smaller amplitude of S -waves. These signatures allow to trace the particular solution in the whole energy range. On the other hand unlike the situation at high energies we saw comparatively small effect of the polarization. In terms of the amplitude analysis it reveals in quite small difference between the barred and unbarred amplitudes. In the limit of zero polarization effect these amplitudes must coincide. So one and the same solution should take place for both sets of amplitudes. From this point of view only solutions 1.1 and 2.2 (in terms of M. Svec [20]) look reasonable.

In both solutions the visible asymmetry is most concentrated in the L -wave. The partial polarization in this wave is $P_L = -0.10 \pm 0.02$. The effects of the spin are also observed in the relative phases. For instance in the solution 1 the relative phase between U and L -waves ($\cos \gamma_{LU}$) differs noticeably from the relative phase between \bar{U} and \bar{L} -waves ($\cos \bar{\gamma}_{LU}$) at $M_{\pi\pi} > 0.75$ GeV.

The difference between the barred and unbarred amplitudes in our data is not large. This makes reasonable to perform a model-dependent amplitude analysis with assumption, that all spin-dependent matrix elements equal zero. The model-dependent analysis allowed to spread the analysis to a wider mass



a)

b)

Fig. 7. Results of the model-independent amplitude analysis. Solution 1 (a) and 2 (b). Notations: open/filled circles/squares — corresponding wave with recoiled nucleon transversity down/up (except N -wave) this work/M. Svec [20]; open crosses/filled stars — corresponding wave intensity this work/M. Svec [20].

region and decrease errors. The resulting amplitudes are shown in fig. 9 and the numeric data is listed in the appendix. We tested that the intensities obtained in the model-dependent analysis coincide within the errors with those obtained in the model-independent one. The same was tested for the mean relative phases.

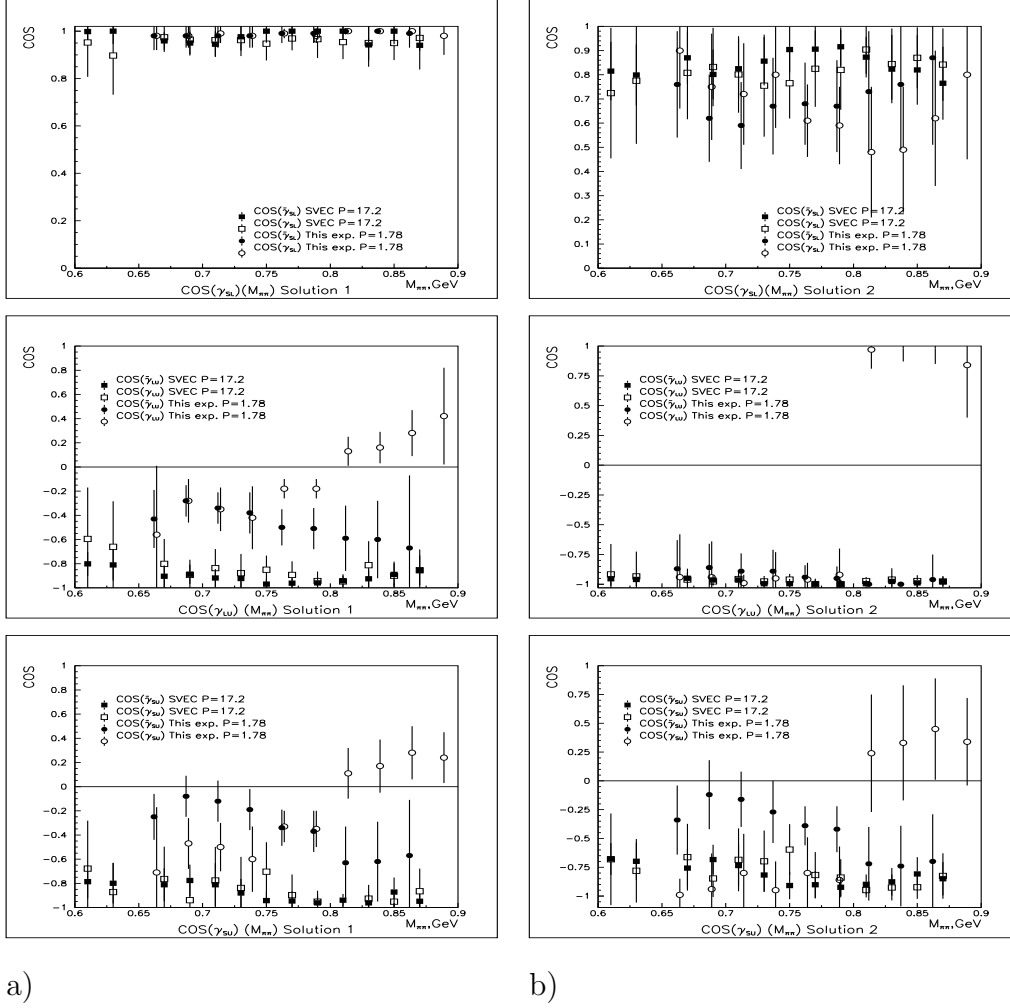


Fig. 8. Results of the model-independent amplitude analysis. Solution 1 (a) and 2 (b). Continued. Notations are the same.

The intensity of the S -wave in the solution 2 is near the intensity of L -wave but the intensities of U and N -waves are abnormally small. In this solution there is also significant energy dependence of relative phase and intensities of S and L -waves. The essential energy dependence of the S -wave intensity in the solution of this type was already noticed by the authors of the analysis [36], performed on the base of the measurements at 4.0 and 4.5 GeV/c [5,36] with bubble chambers. It is difficult to explain all these features of the solution 2 in the frames of the traditional ideas of the mechanism of the peripheral pion production.

Probably, the ambiguity could also be solved in a model-independent way if we complement our experiment with measurements on a longitudinally polarized target. Besides spin-independent SDME such measurement provides three $\text{Im } \rho^z$ components of the spin density matrix:

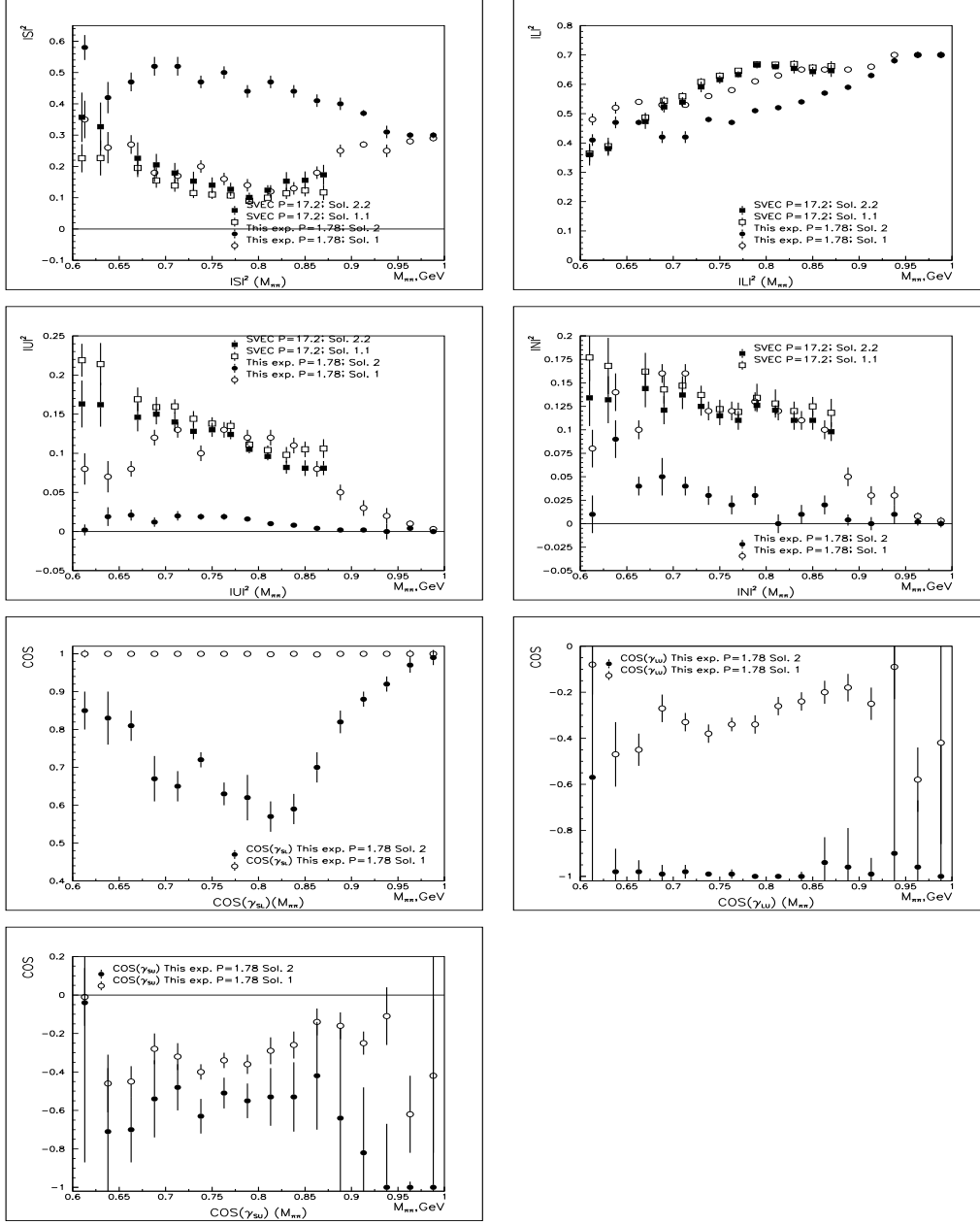


Fig. 9. Results of the model-dependent amplitude analysis. Notations: open/filled circles/squares — solution 1/2 this work/M. Svec [20].

$$\text{Im } \rho_{1S}^z = \frac{1}{\sqrt{2}} \text{Im}(NS^* + \bar{N}\bar{S}^*), \quad (41)$$

$$\text{Im } \rho_{10}^z = \frac{1}{\sqrt{2}} \text{Im}(NL^* + \bar{N}\bar{L}^*), \quad (42)$$

$$\text{Im } \rho_{1-1}^z = -\text{Im}(NU^* + \bar{N}\bar{U}^*), \quad (43)$$

which do not vanish when barred and unbarred amplitudes are equal. The other interesting information, which could be obtained from these measure-

ments is relative phases of N -waves, which are difficult to get from measurements on a transversally polarized target, because of large experimental errors.

In the solution 1 only the relative phase between U and L waves manifests significant energy dependence which should be explained by theory.

6 Evaluation of the parameters of $\sigma(750)$

Both solutions of the amplitude analysis have nearly constant relative $S - L$ -phase and do not have a dip in the ratio I_S/I_L . Yet, in the L -wave a strong ρ -resonance is present. As a consequence there should be a scalar-isoscalar² resonance in S -wave with similar mass and width. In order to estimate its parameters we plotted the unnormalised intensities of S and L -waves using the normalized amplitudes from our model-dependent analysis and the mass dependence of the cross section obtained at 2.26 GeV/c in 4π -geometry experiment [6]. The unnormalised amplitudes were fitted by relativistic Breit-Wigner formula with constant incoherent background:

$$I(m) = qF(m)N(|BW(m)|^2 + B). \quad (44)$$

Here $m = M_{\pi\pi}$ is the invariant mass of dipion, N is a normalizing constant, B is the constant background, $q = \frac{1}{2}\sqrt{m^2 - 4m_\pi^2}$ is the momentum of pions in the dipion rest frame, $BW(m) = \frac{m_R\Gamma}{m_R^2 - m^2 - im_R\Gamma}$ is relativistic Breit-Wigner amplitude [24], $F(m) = (2J + 1)(\frac{m}{q})^2$ is Pišút-Roos resonance shape formula [37]. The mass dependence of the width is given by the equation:

$$\Gamma = \Gamma_R \left(\frac{q}{q_R}\right)^{2J+1} \frac{D_J(q_R r)}{D_J(qr)}. \quad D_J(qr) = \begin{cases} 1 & , J = 0 \\ 1 + (qr)^2 & , J = 1 \end{cases} \text{ is centrifugal barrier}$$

functions of Blatt and Weishopf [38]. And at last m_R and Γ_R are the mass and width of the resonance and q_R is the q at the point $m = m_R$. The fits for S and L -wave intensities in the solution 1 are shown in fig. 10. The description of L -wave gives $M_\rho = 764 \pm 3$ MeV and $\Gamma_\rho = 139 \pm 14$ MeV which is in good agreement with world data over ρ -meson ($M_\rho = 768.5 \pm 0.6$ MeV and $\Gamma_\rho = 150.7 \pm 1.2$ MeV [24]). The results of our fitting to S -wave are shown in tab. 2 together with the data at other energies for the same solution.

The average data over listed 4 estimates of $\sigma(750)$ parameters is:

² The state is symmetrical so it could be only isospin 0 or 2. But the wave with isospin 2 is believed to be small and such a state will have an open exotic, because a meson with isospin 2 can not be combined from quark-anti-quark pair

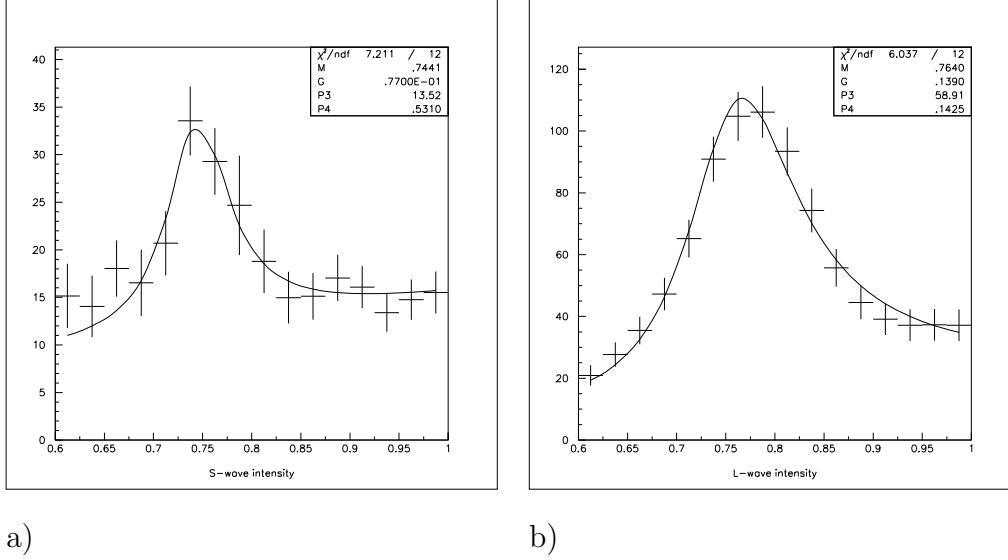


Fig. 10. Breit-Wigner fits for S (a) and L -waves intensities.

Table 2

Parameters of $\sigma(750)$

p_{beam} GeV/c	Mass MeV	Width MeV	Reaction	Experiment	Analysis
1.78	744 ± 5	77 ± 22	$\pi^- p_{\uparrow} \rightarrow \pi^- \pi^+ n$		this work
5.98	746 ± 16	145 ± 69	$\pi^+ n_{\uparrow} \rightarrow \pi^- \pi^+ p$	[12]	[20]
11.85	782 ± 16	117 ± 26	$\pi^+ n_{\uparrow} \rightarrow \pi^- \pi^+ p$	[12]	[20]
17.2	771 ± 13	161 ± 22	$\pi^- p_{\uparrow} \rightarrow \pi^- \pi^+ n$	[11]	[39]

$$M_{\sigma} = 750 \pm 4 \text{ MeV} \quad \chi^2/ndf = 8.11/3 ;$$

$$\Gamma_{\sigma} = 119 \pm 13 \text{ MeV} \quad \chi^2/ndf = 7.44/3 .$$

The available information about the $\sigma(750)$ -meson is quite contradictory. In the last edition of the *Review of Particle Physics* [24] this meson is present as $f_0(400 - 1200)$ with rather unfixed parameters (mass 400–1200 MeV and width 600–1000 MeV). It is seen in a number of works but the situation remains rather unclear. On one hand amplitude analysis of the experimental data obtained on polarized targets supports narrow (70–200 MeV) resonance decaying into two charged pions. On the other hand partial wave analyses of the data from unpolarized targets resulted in a wide weak resonance and its parameters provided by different analyses are much different. The possible reason lays in the approximation of spin-independence used in partial wave analyses. Particularly these analyses disregarded the contribution of the helicity non flip amplitudes. From the experiments performed on polarized targets [11,12] it is known that this approximation is rather strongly violated

especially at high energies, where asymmetry reaches 50%. But it is high energy region where most recent and precise measurements were made. New interesting data concerning the problem of σ -meson could be obtained in the experimental study of the reaction $\pi^- p \rightarrow \pi^0 \pi^0 n$, in which P -wave is forbidden, on a polarized target [40]. This would be a natural continuation of the experiments performed on unpolarized targets by E852-collaboration at 18 GeV/c [41] and by GAMS-collaboration at 38 GeV/c [42]. On the other hand the study of the same reaction at intermediate energies even on unpolarized target is also interesting. Small polarization effects observed in this work at 1.78 GeV/c make believe that correct amplitude analysis could be done without information about spin-dependent SDME.

7 Phenomenological analysis

In this section we want to present some estimates of energy dependence of the amplitudes in the frame of Regge model. This allows to compare our results to those at high energies. It is well known that Regge phenomenology successfully describes energy dependence of amplitudes. Reggitized one pion exchange was successfully used for interpretation of peripheral pion production [36]. We will use the model by Kimel and Owens [27], which takes into account the asymptotically dying amplitudes, that are essential in the range of this experiment, as well as a_1 -exchange amplitudes, which describe the spin dependence of the dynamics of the pion generation. The model was parameterized by the data at 17.2 GeV/c [11,28]. The authors worked with helicity s -channel amplitudes. We used the crossing equations to transfer to the Jackson system used in this work:

$$S_{+\pm} = S_{+\pm}^S, \quad N_{+\pm} = N_{+\pm}^S, \quad (45)$$

$$L_{+\pm} = \cos \chi \cdot L_{+\pm}^S + \sin \chi \cdot U_{+\pm}^S, \quad (46)$$

$$U_{+\pm} = -\sin \chi \cdot L_{+\pm}^S + \cos \chi \cdot U_{+\pm}^S, \quad (47)$$

where χ is the crossing angle of the vector meson and upper script S denotes s -channel helicity amplitudes. The model parameterizes the pion pole terms as:

$$L_{+-}^S = \sqrt{-t'} \cdot \beta_\pi \frac{m_\rho}{2} e^{C_\pi^0(t-m_\pi^2)} \xi_\pi, \quad L_{++}^S = -r L_{+-}^S, \quad (48)$$

$$S_{+\pm}^S = L_{+\pm}^S \Gamma e^{i\Delta}, \quad (49)$$

$$U_{+-}^{SP} = (-t') \cdot \beta_\pi \frac{m_\rho}{2} e^{C_\pi^1(t-m_\pi^2)} \xi_\pi, \quad (50)$$

$$U_{++}^S = -r U_{+-}^{SP}, \quad (51)$$

where $\xi_\pi = \Gamma(-\alpha_\pi)(1 + e^{-i\pi\alpha_\pi})(\frac{s}{s_0})^{\alpha_\pi}$, $\alpha_\pi = 0.7(t - m_\pi^2)$, $r = \sqrt{\frac{t_{\min}}{t'}}$, $\Gamma = 0.4$, $\Delta = 0.4$, $s_0 = 1.0 \text{ GeV}^2$. The pion pole residues correspond to those used in the standard pion exchange model. All the amplitudes written above have common Regge phase independent on the energy. The contribution of the Regge cut is described as:

$$U_{+-}^{SC} = N_{+-}^{SC} = \beta_C e^{C_C t} s^{\alpha_C} e^{i\pi\alpha_C/2}, \quad (52)$$

where $\alpha_C = 0.0 + 0.4t$. At low $|t|$ this provides the relative phase of contributions to U^S - amplitude from cut and pole terms near 180° . The constants β_π , β_C , C_π^0 , C_π^1 and C_C are parameters of the model.

From equations (48-51) one can expect neither the energy dependence in the S to L intensity ratio nor in the relative phase for s -channel transversity amplitudes, though their phases change with decreasing energy, because of increasing contribution of amplitudes without helicity flip S_{++}^S and L_{++}^S , which contain term r . The amplitude U_{+-}^S contains contributions from the pion pole and the cut with opposite signs. At $17.2 \text{ GeV}/c$ it changes its sign at $t' = -0.02 \text{ (GeV}/c)^2$. The pole amplitude U_{+-}^{SP} is decreasing with the decrease of energy because of the growth of minimum momentum transferred. So the point where amplitude U_{+-}^S becomes zero moves to $t' = -0.06 \text{ (GeV}/c)^2$ at $1.78 \text{ GeV}/c$ for $M_{\pi\pi} = 0.77 \text{ GeV}$. From the crossing relations one can see that contributions of the amplitudes L_{++}^S and U_{++}^S , which are taken as a reference point for phases, to the real part $r(-\sin \chi \cdot L_{++}^S + \cos \chi \cdot U_{++}^S)$ of transversity t -channel U -amplitude compensate each other, while there is no compensation of the imaginary part of amplitude, because of the zero in U_{+-}^S . That's why U -amplitude is imaginary at the point $U_{+-}^S = 0$ and the phase of L -amplitude is determined by the parameter r , which is a function of the initial energy. At $r = 1$ and $t' = -0.06 \text{ (GeV}/c)^2$ the estimation of relative phase between U and L -amplitudes basing on the model parameters [27] gives 130° , which is in agreement with the amplitude analysis solution 1 and in contradiction to the solution 2.

Spin dependence of the production process in model [27] is determined by the exchange by the axial-vector meson a_1 ($J^P = 1^+$), which is parameterized as contributions of the Regge pole and cut:

$$L_{++}^P = \beta_{a_1}^0 e^{C_{a_1}^0 t} \xi_{a_1}, \quad L_{++}^C = -i\beta_{a_1}^{a_1} e^{C_{a_1}^{a_1} t} (\frac{s}{s_0})^{\alpha_{a_1}^{a_1}} e^{-i\pi\frac{\alpha_{a_1}^{a_1}}{2}}, \quad (53)$$

where $\xi_{a_1} = \Gamma(1 - \alpha_{a_1})(1 - e^{-i\pi\alpha_{a_1}})(\frac{s}{s_0})^{\alpha_{a_1}^{a_1}}$. The Regge trajectories are given as: $\alpha_{a_1} = -0.3 + 0.9t$ and $\alpha_{a_1}^C = -0.4 + 0.45t$. At small momenta transferred amplitudes L_{++}^P and L_{++}^C have opposite phases and values for $\beta_{a_1}^0$ and $\beta_{a_1}^{a_1}$ fitted at $17.2 \text{ GeV}/c$ satisfy the relation $\beta_{a_1}^0 \approx -\beta_{a_1}^{a_1}$. The partial polarization

of L -wave is defined as:

$$P_L = \frac{2 \operatorname{Im} L_{++}^S \cdot L_{+-}^S}{\sigma}, \quad (54)$$

where σ is the sum of modules squared of the all s -channel amplitudes. Using (53) we can write the energy dependence of the partial polarization in this model:

$$P_L \sim \frac{\left(\frac{s}{s_0}\right)^{\alpha_{a_1}} - \left(\frac{s}{s_0}\right)^{\alpha_C}}{1 + r^2}, \quad (55)$$

because the part of amplitude L_{++}^S , determined by the contribution of pion pole has the same phase as L_{+-}^S and does not contribute to the polarization. Then taking intercept of Regge cut of a_1 from Kimel and Owens we see that the decrease of partial polarization observed $\frac{P_L(17.2)}{P_L(1.78)} = 3.0 \pm 0.7$ correspond to the intercept of Regge trajectory of a_1 -meson -0.1 ± 0.2 and does not contradict to the one, estimated by Kimel and Owens -0.3 ± 0.1 [27].

8 Conclusions

In the experiment presented here all 14 SDME of the reaction (1) were measured for the first time in the resonance region. This allowed us to perform both model-dependent and model-independent amplitude analyses and phenomenological analysis of the data obtained. These analyses lead us to the conclusion that the only physically justified solution of the amplitude analysis is solution 1, which corresponds to the solution "UP" of the $\pi\pi$ partial wave analysis. The clear signature of the solution allows to state that at high energies only solution with minimum S -wave intensity under the peak of ρ -meson is true (solution 1.1 from M. Svec's analysis [20]). We should mention that it is solution 1.1 from all four M. Svec's solutions for the intensity, where resonant behaviour of S -wave is especially clear. This could be an additional argument in favour of the existing of a narrow σ -meson. The mass dependence of S -wave intensity obtained in this work is similar to the one observed at high energies and correspond to existing of narrow ($\Gamma \sim 100$ MeV) S -wave scalar-isoscalar resonance, originally proposed in [12].

The constituent structure of $\sigma(750)$ is still an open question. It is very doubtful that this is a quarkonium state. Hybrid quark-gluonium or pure gluonium nature of the σ -meson looks much more probable. M. Svec, using results of works [43,44], which connected mass and width of gluonium in the frames of low-energy theorems of broken chiral symmetry, proposed that this state could

be a low-energy gluonium. These theorems predict width about 100 MeV for a gluonium with mass 750 MeV, which does not contradict to the experiment. On the other hand quantum chromodynamic calculations on lattices [45,46] set the lowest limits for scalar gluonium mass as 1550 ± 50 and 1740 ± 70 MeV, correspondingly. But earlier works gave the value 740 ± 40 MeV for the mass of the basic state of gluonium [47]. Here we also want to mention an interpretation of light scalar resonances as “new hadrons” or “vacuum scalars” with small width of the decay into two pions. This model beyond standard QCD was recently proposed by V.N. Gribov et al. [48].

The experimental data show the spin dependence of the dipion production dynamics at the level of 6 standard deviations at intermediate energies. The sign of the asymmetry coincides with the one at high energies but the value is (3–4) times smaller. The largest effects are observed in ρ -meson production. Our analysis of the energy dependence of the polarization in the frame of Regge model by Kimel and Owens resulted in a value of a_1 Regge trajectory intercept -0.1 ± 0.2 .

Acknowledges

We are grateful to the ITEP accelerator division for the pion beam production allowing us to conduct these measurements. Authors want to thank V.V. Vladimirkii, A.B. Kaidalov and Yu.S. Kalashnikova for the fruitful discussions of our results. We want to thank M. Svec and R. Kaminski for their comments on their works on scalar mesons and amplitude analysis.

The work was partially supported by the Russian Fund for Basic Research and Russian State Program ”Fundamental Nuclear Physics”.

Table .1

Spin-independent SDME as function of the dipion mass integrated over momentum transferred in the region $0.005 < t_{\min} - t < 0.2$ (GeV/c)².

$M_{\pi\pi}$, MeV	$\rho_{00} + \frac{1}{3}\rho_{SS}$	ρ_{1-1}	Re ρ_{10}	Re ρ_{0S}	Re ρ_{1S}
613	.604 ± .016	.002 ± .010	−.011 ± .017	.413 ± .024	.001 ± .018
638	.611 ± .015	.034 ± .011	−.065 ± .017	.372 ± .028	.045 ± .014
663	.628 ± .010	.009 ± .006	−.069 ± .010	.383 ± .017	.049 ± .008
688	.593 ± .017	.018 ± .008	−.049 ± .011	.314 ± .025	.030 ± .008
713	.591 ± .013	.011 ± .006	−.064 ± .008	.301 ± .018	.035 ± .007
738	.634 ± .008	.007 ± .004	−.066 ± .006	.343 ± .011	.042 ± .004
763	.633 ± .009	−.002 ± .004	−.066 ± .006	.306 ± .013	.035 ± .004
788	.657 ± .008	.007 ± .004	−.064 ± .006	.294 ± .027	.033 ± .004
813	.673 ± .011	−.004 ± .004	−.051 ± .007	.283 ± .021	.026 ± .006
838	.689 ± .013	.000 ± .004	−.046 ± .008	.290 ± .021	.022 ± .006
863	.707 ± .013	.007 ± .004	−.032 ± .008	.337 ± .018	.012 ± .006
888	.727 ± .010	.001 ± .003	−.024 ± .008	.399 ± .013	.013 ± .006
913	.754 ± .008	−.002 ± .003	−.027 ± .007	.425 ± .008	.017 ± .004
938	.785 ± .009	.005 ± .003	−.007 ± .011	.421 ± .011	.005 ± .007
963	.797 ± .007	−.001 ± .002	−.034 ± .007	.442 ± .006	.023 ± .004
988	.799 ± .009	.000 ± .002	−.014 ± .010	.453 ± .007	.009 ± .006

Table .2

Spin-independent SDME as function of the momentum transferred $-t' = t - t_{\min}$ integrated over dipion mass in the region $700 < M_{\pi\pi} < 850$ MeV.

$-t', (\text{GeV}/c)^2$	$\rho_{00} + \frac{1}{3}\rho_{SS}$	ρ_{1-1}	$\text{Re } \rho_{10}$	$\text{Re } \rho_{0S}$	$\text{Re } \rho_{1S}$
.002	$.600 \pm .025$	$.016 \pm .008$	$-.035 \pm .016$	$.220 \pm .035$	$.022 \pm .018$
.007	$.620 \pm .025$	$-.004 \pm .007$	$-.045 \pm .010$	$.250 \pm .025$	$.027 \pm .014$
.012	$.600 \pm .025$	$-.009 \pm .007$	$-.075 \pm .010$	$.260 \pm .035$	$.044 \pm .008$
.017	$.620 \pm .025$	$-.012 \pm .010$	$-.085 \pm .016$	$.190 \pm .040$	$.040 \pm .008$
.025	$.610 \pm .025$	$.000 \pm .007$	$-.069 \pm .010$	$.245 \pm .025$	$.043 \pm .007$
.035	$.620 \pm .025$	$.003 \pm .007$	$-.069 \pm .010$	$.250 \pm .025$	$.035 \pm .004$
.045	$.640 \pm .020$	$.027 \pm .007$	$-.070 \pm .010$	$.265 \pm .025$	$.037 \pm .004$
.055	$.615 \pm .020$	$.027 \pm .010$	$-.071 \pm .012$	$.230 \pm .035$	$.032 \pm .004$
.070	$.630 \pm .020$	$.041 \pm .007$	$-.078 \pm .008$	$.295 \pm .025$	$.033 \pm .006$
.090	$.625 \pm .020$	$.047 \pm .010$	$-.095 \pm .010$	$.280 \pm .025$	$.037 \pm .006$

Table .3

Spin-dependent SDME integrated over momentum transferred in the region $0.005 < t_{\min} - t < 0.2$ $(\text{GeV}/c)^2$.

$M_{\pi\pi},$ GeV	$A = \rho_{SS}^Y +$ $\rho_{00}^Y + 2\rho_{11}^Y$	$\rho_{00}^Y - \rho_{11}^Y$	ρ_{1-1}^Y	$\text{Re } \rho_{10}^Y$	$\text{Re } \rho_{0S}^Y$	$\text{Re } \rho_{1S}^Y$	$\text{Im } \rho_{0S}^X$	$\text{Im } \rho_{10}^X$	$\text{Im } \rho_{1S}^X$
.65-.75	$-.07 \pm .16$	$-.09 \pm .08$	$.008 \pm .025$	$.007 \pm .016$	$.00 \pm .07$	$-.022 \pm .016$	$.018 \pm .025$	$.025 \pm .020$	$.022 \pm .016$
.75-.80	$-.11 \pm .11$	$-.03 \pm .07$	$-.034 \pm .028$	$.031 \pm .011$	$-.02 \pm .06$	$.000 \pm .011$	$-.017 \pm .028$	$.059 \pm .016$	$.028 \pm .011$
.80-.90	$-.26 \pm .18$	$-.28 \pm .13$	$.00 \pm .03$	$.073 \pm .018$	$-.12 \pm .08$	$.034 \pm .013$	$.04 \pm .03$	$.034 \pm .018$	$.017 \pm .013$

Table .4

Model-independent analysis. t -channel transversity amplitudes as function of the dipion mass. Solution 1.

$M_{\pi\pi}$, MeV	$ S ^2$	$ L ^2$	$ \bar{N} ^2$	$ U ^2$	$\cos \gamma_{LS}$	$\cos \gamma_{LU}$	$\cos \gamma_{SU}$
663	$.18 \pm .09$	$.21 \pm .06$	$.05 \pm .05$	$.03 \pm .05$	$.98 \pm .06$	$-.56 \pm .57$	$-.71 \pm .54$
688	$.12 \pm .07$	$.21 \pm .05$	$.08 \pm .04$	$.05 \pm .04$	$.98 \pm .05$	$-.28 \pm .18$	$-.47 \pm .21$
713	$.11 \pm .06$	$.22 \pm .05$	$.08 \pm .04$	$.06 \pm .04$	$.99 \pm .04$	$-.35 \pm .18$	$-.50 \pm .20$
738	$.13 \pm .07$	$.23 \pm .05$	$.06 \pm .04$	$.04 \pm .04$	$.98 \pm .05$	$-.42 \pm .26$	$-.60 \pm .27$
763	$.08 \pm .04$	$.26 \pm .04$	$.03 \pm .03$	$.07 \pm .03$	$.99 \pm .02$	$-.18 \pm .08$	$-.33 \pm .13$
788	$.07 \pm .04$	$.28 \pm .03$	$.04 \pm .03$	$.06 \pm .03$	$.98 \pm .03$	$-.18 \pm .08$	$-.35 \pm .15$
813	$.04 \pm .04$	$.19 \pm .06$	$.07 \pm .04$	$.08 \pm .04$	$1.00 \pm .005$	$.13 \pm .12$	$.11 \pm .21$
838	$.04 \pm .04$	$.20 \pm .06$	$.07 \pm .04$	$.07 \pm .04$	$1.00 \pm .001$	$.16 \pm .13$	$.17 \pm .22$
863	$.06 \pm .05$	$.20 \pm .06$	$.06 \pm .04$	$.05 \pm .04$	$1.00 \pm .002$	$.28 \pm .19$	$.28 \pm .22$
888	$.10 \pm .10$	$.19 \pm .07$	$.04 \pm .05$	$.04 \pm .05$	$.98 \pm .08$	$.42 \pm .40$	$.24 \pm .21$

Table .5

Model-independent analysis. t -channel transversity amplitudes as function of the dipion mass. Solution 2.

$M_{\pi\pi}$, MeV	$ S ^2$	$ L ^2$	$ \bar{N} ^2$	$ U ^2$	$\cos \gamma_{LS}$	$\cos \gamma_{LU}$	$\cos \gamma_{SU}$
663	$.23 \pm .11$	$.20 \pm .04$	$.03 \pm .03$	$.011 \pm .006$	$.90 \pm .24$	$-.94 \pm .36$	$-.99 \pm .14$
688	$.26 \pm .10$	$.17 \pm .04$	$.03 \pm .03$	$.006 \pm .004$	$.75 \pm .22$	$-.94 \pm .30$	$-.94 \pm .31$
713	$.26 \pm .10$	$.17 \pm .04$	$.03 \pm .03$	$.010 \pm .006$	$.72 \pm .21$	$-.99 \pm .07$	$-.80 \pm .34$
738	$.23 \pm .10$	$.20 \pm .04$	$.02 \pm .03$	$.010 \pm .004$	$.80 \pm .22$	$-.95 \pm .22$	$-.95 \pm .25$
763	$.28 \pm .08$	$.19 \pm .04$	$.03 \pm .03$	$.003 \pm .002$	$.61 \pm .15$	$-.96 \pm .14$	$-.80 \pm .31$
788	$.25 \pm .08$	$.22 \pm .04$	$.00 \pm .03$	$.003 \pm .002$	$.59 \pm .16$	$-.92 \pm .22$	$-.86 \pm .29$
813	$.25 \pm .12$	$.12 \pm .07$	$.00 \pm .03$	$.002 \pm .004$	$.48 \pm .27$	$.97 \pm .16$	$.24 \pm .51$
838	$.23 \pm .12$	$.13 \pm .07$	$.00 \pm .03$	$.003 \pm .005$	$.49 \pm .26$	$.98 \pm .11$	$.33 \pm .50$
863	$.20 \pm .12$	$.15 \pm .06$	$.01 \pm .03$	$.006 \pm .007$	$.62 \pm .28$	$.98 \pm .13$	$.45 \pm .44$
888	$.18 \pm .13$	$.17 \pm .06$	$.01 \pm .03$	$.010 \pm .020$	$.80 \pm .35$	$.84 \pm .44$	$.34 \pm .38$

Table .6

Model-independent analysis. t -channel transversity amplitudes as function of the dipion mass. Solution 1.

$M_{\pi\pi}$, MeV	$ \bar{S} ^2$	$ \bar{L} ^2$	$ N ^2$	$ \bar{U} ^2$	$\cos \bar{\gamma}_{LS}$	$\cos \bar{\gamma}_{LU}$	$\cos \bar{\gamma}_{SU}$
663	$.12 \pm .06$	$.32 \pm .05$	$.05 \pm .04$	$.05 \pm .04$	$.98 \pm .06$	$-.43 \pm .24$	$-.25 \pm .19$
688	$.08 \pm .05$	$.31 \pm .05$	$.08 \pm .04$	$.07 \pm .04$	$.98 \pm .05$	$-.28 \pm .13$	$-.08 \pm .17$
713	$.08 \pm .04$	$.31 \pm .04$	$.08 \pm .04$	$.07 \pm .04$	$.98 \pm .05$	$-.34 \pm .13$	$-.12 \pm .17$
738	$.08 \pm .05$	$.33 \pm .05$	$.06 \pm .04$	$.06 \pm .04$	$.98 \pm .05$	$-.38 \pm .17$	$-.19 \pm .17$
763	$.09 \pm .04$	$.32 \pm .04$	$.09 \pm .03$	$.06 \pm .03$	$.99 \pm .04$	$-.50 \pm .15$	$-.34 \pm .15$
788	$.08 \pm .04$	$.33 \pm .04$	$.09 \pm .03$	$.05 \pm .03$	$.99 \pm .04$	$-.51 \pm .17$	$-.37 \pm .17$
813	$.09 \pm .04$	$.44 \pm .06$	$.05 \pm .04$	$.05 \pm .04$	$.999 \pm .013$	$-.59 \pm .27$	$-.63 \pm .30$
838	$.09 \pm .04$	$.45 \pm .06$	$.04 \pm .04$	$.04 \pm .04$	$1.000 \pm .008$	$-.60 \pm .32$	$-.62 \pm .33$
863	$.12 \pm .06$	$.45 \pm .06$	$.03 \pm .05$	$.03 \pm .05$	$.99 \pm .06$	$-.67 \pm .60$	$-.57 \pm .46$

Table .7

Model-independent analysis. t -channel transversity amplitudes as function of the dipion mass. Solution 2.

$M_{\pi\pi}$, MeV	$ \bar{S} ^2$	$ \bar{L} ^2$	$ N ^2$	$ \bar{U} ^2$	$\cos \bar{\gamma}_{LS}$	$\cos \bar{\gamma}_{LU}$	$\cos \bar{\gamma}_{SU}$
663	$.23 \pm .11$	$.28 \pm .04$	$.01 \pm .03$	$.014 \pm .011$	$.76 \pm .22$	$-.87 \pm .24$	$-.34 \pm .30$
688	$.26 \pm .10$	$.25 \pm .04$	$.02 \pm .03$	$.009 \pm .008$	$.62 \pm .18$	$-.86 \pm .20$	$-.12 \pm .30$
713	$.25 \pm .10$	$.25 \pm .04$	$.02 \pm .03$	$.013 \pm .008$	$.59 \pm .18$	$-.89 \pm .15$	$-.16 \pm .24$
738	$.23 \pm .10$	$.28 \pm .04$	$.01 \pm .03$	$.012 \pm .008$	$.67 \pm .20$	$-.89 \pm .18$	$-.27 \pm .27$
763	$.21 \pm .08$	$.27 \pm .04$	$.05 \pm .03$	$.019 \pm .007$	$.68 \pm .17$	$-.94 \pm .10$	$-.39 \pm .17$
788	$.19 \pm .08$	$.30 \pm .04$	$.06 \pm .03$	$.017 \pm .006$	$.67 \pm .19$	$-.95 \pm .10$	$-.42 \pm .20$
813	$.19 \pm .12$	$.41 \pm .06$	$.01 \pm .03$	$.019 \pm .006$	$.73 \pm .25$	$-1.00 \pm .005$	$-.72 \pm .32$
838	$.17 \pm .12$	$.42 \pm .06$	$.02 \pm .03$	$.017 \pm .006$	$.76 \pm .27$	$-1.00 \pm .01$	$-.74 \pm .35$
863	$.16 \pm .12$	$.44 \pm .07$	$.02 \pm .03$	$.014 \pm .009$	$.87 \pm .36$	$-.96 \pm .21$	$-.70 \pm .41$

Table .8

Model-dependent analysis. t -channel transversity amplitudes as function of the dipion mass. Solution 1.

$M_{\pi\pi}$, MeV	I_S	I_L	I_N	I_U	$\cos \gamma_{LS}$	$\cos \gamma_{LU}$	$\cos \gamma_{SU}$
613	$.35 \pm .06$	$.48 \pm .02$	$.08 \pm .02$	$.08 \pm .02$	$1.00 \pm .01$	$-.08 \pm .13$	$-.01 \pm .15$
638	$.26 \pm .05$	$.52 \pm .02$	$.14 \pm .02$	$.07 \pm .02$	$1.000 \pm .003$	$-.47 \pm .14$	$-.46 \pm .15$
663	$.27 \pm .03$	$.54 \pm .01$	$.10 \pm .01$	$.08 \pm .01$	$1.000 \pm .001$	$-.45 \pm .07$	$-.45 \pm .08$
688	$.18 \pm .03$	$.53 \pm .02$	$.16 \pm .01$	$.12 \pm .01$	$1.000 \pm .001$	$-.27 \pm .06$	$-.28 \pm .08$
713	$.17 \pm .02$	$.53 \pm .01$	$.16 \pm .01$	$.13 \pm .01$	$1.000 \pm .001$	$-.33 \pm .04$	$-.32 \pm .07$
738	$.20 \pm .02$	$.56 \pm .01$	$.12 \pm .01$	$.10 \pm .01$	$1.000 \pm .001$	$-.38 \pm .04$	$-.40 \pm .04$
763	$.16 \pm .02$	$.58 \pm .01$	$.12 \pm .01$	$.13 \pm .01$	$1.000 \pm .001$	$-.34 \pm .03$	$-.34 \pm .04$
788	$.14 \pm .02$	$.61 \pm .01$	$.13 \pm .01$	$.12 \pm .01$	$1.000 \pm .002$	$-.34 \pm .04$	$-.36 \pm .05$
813	$.12 \pm .02$	$.63 \pm .01$	$.12 \pm .01$	$.12 \pm .01$	$.999 \pm .003$	$-.26 \pm .04$	$-.29 \pm .07$
838	$.13 \pm .02$	$.65 \pm .01$	$.11 \pm .01$	$.11 \pm .01$	$1.000 \pm .001$	$-.24 \pm .04$	$-.26 \pm .07$
863	$.18 \pm .02$	$.65 \pm .01$	$.10 \pm .01$	$.08 \pm .01$	$.998 \pm .005$	$-.20 \pm .05$	$-.14 \pm .07$
888	$.25 \pm .02$	$.65 \pm .01$	$.05 \pm .01$	$.05 \pm .01$	$1.000 \pm .002$	$-.18 \pm .06$	$-.16 \pm .07$
913	$.27 \pm .01$	$.66 \pm .01$	$.03 \pm .01$	$.03 \pm .01$	$1.000 \pm .001$	$-.25 \pm .07$	$-.25 \pm .06$
938	$.25 \pm .02$	$.70 \pm .01$	$.03 \pm .01$	$.02 \pm .01$	$1.000 \pm .003$	$-.09 \pm .14$	$-.11 \pm .15$
963	$.28 \pm .01$	$.70 \pm .01$	$.008 \pm .004$	$.010 \pm .004$	$1.00 \pm .01$	$-.58 \pm .14$	$-.62 \pm .20$
988	$.29 \pm .01$	$.70 \pm .01$	$.003 \pm .004$	$.003 \pm .004$	$1.000 \pm .002$	$-.42 \pm .44$	$-.42 \pm .40$

Table .9

Model-dependent analysis. t -channel transversity amplitudes as function of the dipion mass. Solution 2.

$M_{\pi\pi}$, MeV	I_S	I_L	I_N	I_U	$\cos \gamma_{LS}$	$\cos \gamma_{LU}$	$\cos \gamma_{SU}$
613	$.58 \pm .04$	$.41 \pm .02$	$.01 \pm .02$	$.002 \pm .007$	$.85 \pm .05$	$-.57 \pm .70$	$-.04 \pm .83$
638	$.42 \pm .05$	$.47 \pm .02$	$.09 \pm .02$	$.019 \pm .012$	$.83 \pm .07$	$-.98 \pm .10$	$-.71 \pm .33$
663	$.47 \pm .03$	$.47 \pm .01$	$.04 \pm .01$	$.021 \pm .007$	$.81 \pm .04$	$-.98 \pm .05$	$-.70 \pm .17$
688	$.52 \pm .03$	$.42 \pm .02$	$.05 \pm .02$	$.012 \pm .006$	$.67 \pm .06$	$-.99 \pm .04$	$-.54 \pm .20$
713	$.52 \pm .03$	$.42 \pm .02$	$.04 \pm .01$	$.020 \pm .006$	$.65 \pm .04$	$-.98 \pm .03$	$-.48 \pm .12$
738	$.47 \pm .02$	$.48 \pm .01$	$.03 \pm .01$	$.019 \pm .004$	$.72 \pm .02$	$-.99 \pm .01$	$-.63 \pm .09$
763	$.50 \pm .02$	$.47 \pm .01$	$.02 \pm .01$	$.019 \pm .004$	$.63 \pm .03$	$-.99 \pm .02$	$-.51 \pm .08$
788	$.44 \pm .02$	$.51 \pm .01$	$.03 \pm .01$	$.016 \pm .003$	$.62 \pm .06$	$-1.00 \pm .01$	$-.55 \pm .09$
813	$.47 \pm .02$	$.52 \pm .01$	$.00 \pm .01$	$.010 \pm .003$	$.57 \pm .04$	$-1.00 \pm .01$	$-.53 \pm .15$
838	$.44 \pm .02$	$.54 \pm .01$	$.01 \pm .01$	$.008 \pm .003$	$.59 \pm .04$	$-1.00 \pm .02$	$-.53 \pm .18$
863	$.41 \pm .02$	$.57 \pm .01$	$.02 \pm .01$	$.004 \pm .003$	$.70 \pm .04$	$-.94 \pm .11$	$-.42 \pm .28$
888	$.40 \pm .02$	$.59 \pm .01$	$.004 \pm .006$	$.002 \pm .002$	$.82 \pm .03$	$-.96 \pm .17$	$-.64 \pm .47$
913	$.37 \pm .01$	$.63 \pm .01$	$.000 \pm .007$	$.002 \pm .001$	$.88 \pm .02$	$-.99 \pm .07$	$-.82 \pm .34$
938	$.31 \pm .02$	$.68 \pm .01$	$.01 \pm .01$	$.00 \pm .01$	$.92 \pm .02$	$-.91 \pm .8$	$-1.00 \pm .33$
963	$.30 \pm .01$	$.70 \pm .01$	$.002 \pm .004$	$.004 \pm .001$	$.97 \pm .02$	$-.96 \pm .29$	$-1.00 \pm .03$
988	$.30 \pm .01$	$.70 \pm .01$	$.000 \pm .004$	$.000 \pm .001$	$.99 \pm .02$	$-1.00 \pm .57$	-1.00 ± 1.4

References

- [1] L.D. Jacobs et al., *Phys. Rev.* **D6** (1972) 1291.
- [2] B. Haber et al., *Phys. Rev.* **D10** (1974) 1387.
- [3] A.B. Wicklund et al., *Phys. Rev.* **D17** (1978) 1197.
- [4] G.A. Laksin *Uspehi Fizicheskikh Nauk* **102-3** (1970) 337;
A.V. Arefyev et al., *Yadernaya Fizika* **27** (1964) 161.
- [5] J.A. Charlesworth et al., *Nucl. Phys.* **B65** (1973) 253.
- [6] B.G. Reynolds et al., *Phys. Rev.* **184** (1969) 1424.
- [7] T.C. Bacon et al., *Phys. Rev.* **157** (1967) 1263.
- [8] W. Ochs and F. Wagner, *Phys. Lett.* **44B** (1973) 271.
- [9] A.B. Kaydalov and B.M. Karnakov, *Yadernaya Fizika* **11** (1970) 216;
B.M. Guzhavin, A.B. Kaydalov and A.F. Nilov, *Yadernaya Fizika* **15** (1972) 162.
- [10] I.G. Alekseev et al., *πN Newsletter* **6** (1992) 35;
I.G. Alekseev et al., *Yad. Fiz.* **55** (1992) 1912.
- [11] H. Becker et al., *Nucl. Phys.* **B150** (1979) 301;
H. Becker et al., *Nucl. Phys.* **B151** (1979) 46.
- [12] A. de Lesquen et al., *Phys. Rev.* **D32** (1985) 21;
A. de Lesquen et al., *Phys. Rev.* **D39** (1989) 21;
A. de Lesquen et al., *Phys. Rev.* **D42** (1990) 934;
A. de Lesquen et al., *Phys. Rev.* **D45** (1992) 55;
A. de Lesquen et al., *Phys. Rev.* **D46** (1992) 949.
- [13] G. Lutz and K. Rybitcki, Max Planck Institute, Munich, Internal Report No. MPI-PAE/Exp. EI.75, 1978 (unpublished).
- [14] K.N. Muhin and O.O. Patarakin, *Uspehi Fizicheskikh Nauk* **133** (1981) 377.
- [15] P.K. Williams, *Phys. Rev.* **D1** (1970) 1312.
- [16] S.M. Roy, *Phys. Rev.* **B36** (1971) 353.
- [17] O.O. Patarakin, V.N. Tihonov and K.N. Muhin, *Nucl. Phys.* **A598** (1996) 335.
- [18] N.M. Cason et al., *Phys. Rev.* **D28** (1983) 1586; and references 12-19 therein
- [19] C. Amsler et al., *Phys. Lett.* **B342** (1995) 433;
C. Amsler et al., *Phys. Lett.* **B355** (1995) 425.
- [20] M. Svec, *Phys. Rev.* **D53** (1996) 2343;
M. Svec, *Phys. Rev.* **D55** (1997) 5727;
M. Svec, **hep-ph/9707495**.

- [21] J.T. Donohue and Y. Leroyer, *Nucl. Phys.* **B158** (1979) 123.
- [22] R. Kaminski, L. Les'niak and K. Rybicky, *Zeit. F. Phys.* **C74** (1997) 79.
- [23] M. Gell-Mann and M. Levy, *Nuovo Cim.* **16** (1960) 705.
- [24] Review of Particle Physics, *Phys. Rev.* **D54** (1996) 1.
- [25] E. Byckling and K. Kajantie, *Particle Kinematics*, John Wiley and Sons, London 1973.
- [26] K. Gotfried and J.D. Jackson, *Nuovo Cim.* **34** (1964) 735;
J.D. Jackson, *Nuovo Cim.* **34** (1964) 1644.
- [27] J.D. Kimel and J.F. Owens, *Nucl. Phys.* **B122** (1977) 464.
- [28] B. Hyams et al., *Nucl. Phys.* **B64** (1973) 134;
G. Grayer et al., *Nucl. Phys.* **B75** (1974) 189;
- [29] I.G. Alekseev et al., *Nucl. Phys.* **B348** (1991) 257.
- [30] I.G. Alekseev et al., Preprint ITEP 184-88, Moscow 1988.
- [31] H. Eichinger and M. Regler, *Review of track fitting methods in counter experiments*, Book CERN 81-06, Geneva 1981.
- [32] F.T. Solmitz, *Annu. Rev. Nucl. Sci.* **14** (1964) 375;
J. Bystricky et al., *Nuovo Cim.* **A1** (1971) 601.
- [33] R. Brun, *GEANT user guide and reference manual*, CERN DD/78/2, 1978.
- [34] I.M. Sobol, *Monte-Carlo Numerical Methods*, Moscow, Nauka, 1973.
- [35] M. Babou et al., *Nucl. Instrum. Methods* **160** (1979) 1.
- [36] A.F. Nilov et al., *Yadernaya Fizika* **22** (1975) 116.
- [37] J. Pišút and M. Roos, *Nucl. Phys.* **B6** (1968) 325.
- [38] J.M. Blatt and V.F. Weiskopf, *Theoretical Nuclear Physics*, New-York, Wiley&Sons, 1952.
- [39] M. Svec, **hep-ph/9707495**.
- [40] M. Svec, **hep-ph/9608339**.
- [41] B.B. Brabson et al., Proc. of Hadron'95, Manchester 1995, World Scientific, 1996, p. 494.
- [42] D. Alde et al., *Z. Phys.* **C66** (1995) 375;
A.A. Kondashov et al., Proc. of the 28th International Conference on High Energy Physics, Warsaw, 1996, p. 474.
- [43] J. Ellis and J. Lanik, *Phys. Lett.* **B150** (1985) 249.

- [44] M.S. Shifman et al., *Nucl. Phys.* **B147** (1979) 385, 448.
- [45] G. Bali et al., *Phys. Lett.* **B309** (1993) 378.
- [46] F. Butler et al., *Phys. Rev. Lett.* **70** (1993) 2849;
M. Chen et al., *Nucl. Phys. (suppl.)* **34** (1994) 357.
- [47] K. Ishikawa et al., *Phys. Lett.* **116B** (1982) 429;
B. Berg and A. Billoire, *Nucl. Phys.* **B221** (1983) 109;
W.H. Hamber and M. Urs Mceiller, *Phys. Rev.* **D29** (1984) 928.
- [48] F.E. Close et al., *Phys. Lett.* **B319** (1993) 291.